Lipid Mixing and Content Release in Single-Vesicle, SNARE-Driven Fusion Assay with 1–5 ms Resolution

Tingting Wang,[†] Elizabeth A. Smith,[‡] Edwin R. Chapman,[§] and James C. Weisshaar[†‡*]
[†]Department of Chemistry, [‡]Graduate Biophysics Program, and [§]Howard Hughes Medical Institute, Department of Physiology, University of Wisconsin, Madison, Wisconsin

ABSTRACT A single-vesicle, fluorescence-based, SNARE-driven fusion assay enables simultaneous measurement of lipid mixing and content release with 5 ms/frame, or even 1 ms/frame, time resolution. The v-SNARE vesicles, labeled with lipid and content markers of different color, dock and fuse with a planar t-SNARE bilayer supported on glass. A narrow (<5 ms duration), intense spike of calcein fluorescence due to content release and dequenching coincides with inner-leaflet lipid mixing within 10 ms. The spike provides more sensitive detection of productive hemifusion events than do lipid labels alone. Consequently, many fast events previously thought to be prompt, full fusion events are now reclassified as productive hemifusion. Both full fusion and hemifusion occur with a time constant of 5–10 ms. At 60% phosphatidylethanolamine lipid composition, productive and dead-end hemifusion account for 65% of all fusion events. However, quantitative analysis shows that calcein is released into the space above the bilayer (vesicle bursting), rather than the thin aqueous space between the bilayer and glass. Evidently, at the instant of inner-leaflet mixing, flattening of the vesicle increases the internal pressure beyond the bursting point. This may be related to in vivo observations suggesting that membrane lysis often competes with membrane fusion.

INTRODUCTION

Membrane fusion plays a central role in many important cellular processes, including protein and lipid trafficking, viral infection of host cells, and exocytosis, the transport of content from vesicle lumen to cell exterior. In an effort to understand the molecular mechanism of exocytosis, a variety of in vitro fusion assays have been devised to monitor either the exchange of lipid labels between the two bilayers or the transport of content across the bilayers, or both (1–3). Protein-free lipid bilayer fusion of 30–150 nm diameter phospholipid vesicles is an exceedingly slow, high-barrier process at 25–37°C (4). Exocytosis in vivo is regulated and greatly accelerated by specialized proteins (5–8). In fast neuronal systems, the population of synaptic vesicles decays on a submillisecond timescale after stimulation by Ca^{2+} (9). Soluble *N*-ethylmaleimide-sensitive-factor attachment protein receptor (SNARE) complexes (10–13) are unusually stable four-helix bundles that comprise the v-SNARE synaptobrevin (syb) anchored in the vesicle membrane and the binary t-SNARE (syntaxin (syx) and SNAP-25) anchored in the target plasma membrane. Formation of SNARE complexes is widely believed to catalyze neuronal exocytosis, but the detailed mechanism remains sketchy (5,14–16).

Protein-free fusion can be driven to occur on a timescale of tens of minutes by osmotic effects, by crowding due to high concentrations of added polymer, or, in the case of anionic lipids, by addition of divalent cations (4,17–19). An approach using a vesicle-plus-planar bilayer geometry (20–25) enables the study of individual fusion events. In one example, investigators simultaneously used transbilayer conductance arising from incorporation of porin channels to monitor lipid mixing, and dequenching of calcein fluorescence to monitor content release with 33-ms time resolution (26). Some events showed both lipid mixing and proper content transfer. However, in many events the vesicle ''burst'' (i.e., released its content to the wrong compartment without incorporating channels into the planar bilayer). In a more recent study, researchers simultaneously monitored hemifusion and content release by following lipid and content labels (27). Both hemifusion and full fusion were observed.

Recently, in vitro fusion assays have been used in an attempt to mimic SNARE-driven vesicle fusion, including the triggering of fusion by Ca^{2+} (12,28,29). The kinetics of SNARE-driven lipid mixing varies with specific experimental conditions, such as lipid composition, protein content, method of reconstitution, and bilayer geometry. The fastest population kinetics for SNARE-driven, Ca^{2+}-triggered vesicle-vesicle fusion still have a time constant of a few minutes, which is much slower than the low- or submillisecond timescales observed in neuronal exocytosis (30).

Several groups have developed SNARE-driven, single-vesicle fusion assays in the vesicle-plus-planar bilayer geometry (31–34). This enables clean separation of docking and fusion events, and a rigorous analysis of the kinetics of both. In a similar spirit, Yoon and co-workers (35,36) monitored single vesicle-vesicle fusion events by immobilizing vesicles on a polyethylene glycol-coated glass slide. Thus far, we have used widefield fluorescence microscopy and

Submitted November 19, 2008, and accepted for publication February 24, 2009.

*Correspondence: weisshaar@chem.wisc.edu

Editor: Edward H. Egelman.

0006-3495/09/05/4122/10 $2.00

doi: 10.1016/j.bpj.2009.02.050

fluorescent lipid labels to monitor single full fusion (32) and hemifusion (31) events for v-SNARE vesicles interacting with a planar t-SNARE bilayer supported on glass. Hemifusion was detected as two successive waves of lipids outwardly diffusing from the point of docking and fusion. It was clearly shown that SNARE-driven hemifusion is often productive, i.e., that the hemifusion state is an intermediate on the path to complete fusion. In contrast to all the other studies, both full fusion and hemifusion were remarkably fast, occurring on a ~25–100 ms timescale. The fraction of hemifusion events was enhanced by addition of the negatively curved lipid component 1,2-dioleoyl-*sn*-glycero-3-phosphoethanolamine (DOPE).

In this study we extend the time resolution of lipid- and content-mixing fluorescence measurements into the 1–5 ms regime during single-vesicle docking and fusion events. We find that prompt, full fusion and hemifusion events are even faster than previously estimated, occurring primarily on a 5–10 ms timescale. Content release, as measured by dequenching of fluorescent calcein, provides a much more sensitive signal of inner-leaflet mixing (core fusion) events than dequenching of lipid labels alone. Many events previously classified as prompt, full fusion are in fact fast, productive hemifusion events, i.e., ''on-path'' hemifusion is even more important in our assay than previously inferred.

However, by quantitatively fitting the time-dependent content intensity profile, we demonstrate that the content is always released into the three-dimensional (3D) space above the planar bilayer. Content release occurs simultaneously with inner-leaflet mixing (core fusion) within 10 ms, but the content is evidently not transmitted into the thin, 1–3 nm water layer between the glass substrate and the planar bilayer as it would be in a proper fusion event. As discussed below, such ''bursting'' behavior may be related to in vivo and in vitro observations suggesting that in the presence of bilayer-disrupting proteins such as the SNAREs, membrane lysis competes with membrane fusion in such diverse systems as yeast vacuole fusion, fusion of mating yeast cells, and virus-liposome fusion (37).

MATERIALS AND METHODS

Vesicle and bilayer preparation

Details of the v-SNARE and t-SNARE proteins and the synthetic lipids used to produce vesicles are given in the Supporting Material and in earlier literature (29,32). The t-SNARE vesicles and content-free v-SNARE vesicles were reconstituted by comicellization followed by rapid dilution and dialysis, and subsequently purified by flotation in an Accudenz (Accurate Chemical, Westbury, NY) step gradient (29). The process yields vesicles of mean diameter 50 nm but with a broad size distribution. The mean protein content was ~0.8 t-SNARE copies/vesicle, as described previously (29). The lipid composition of the t-SNARE vesicles was 15% 1,2-dioleoyl-*sn*-glycero-3-phospho-L-serine (DOPS) and 85% 1-palmitoyl-2-oleoyl-*sn*-glycero-3-phosphocholine (POPC) (mol/mol).

Doubly labeled v-SNARE vesicles were reconstituted by comicellization followed by rapid dilution. The protein content was ~80 v-SNARE copies/vesicle. To label the v-SNARE vesicle content, 50 mM calcein was included in both elution buffer and dialysis buffer during the reconstitution procedures. The v-SNARE vesicles do not leak calcein content for at least 2 days when stored at 4°C after preparation. All v-SNARE vesicles were reconstituted with 15% DOPS. For those without DOPE, the total percentage of POPC plus lipid probes was 85%. For those with 30% DOPE, the total percentage of POPC plus lipid probes was 55%. For those with 60% DOPE, the total percentage of POPC plus lipid probes was 25%. The lipid labels octadecyl rhodamine B (R18) and Texas Red-labeled 1,2-dihexadecanoyl-*sn*-glycero-3-phosphoethanolamine (Texas Red-DHPE) were used at 5% to obtain strong dequenching/polarization enhancement of fluorescence intensity after fusion (32). *N*-(6-tetramethylrhodaminethiocarbamoyl)-1,2-dihexadecanoyl-*sn*-glycero-3-phosphoethanolamine (TRITC-DHPE) at only 1% produced a similar enhancement.

Supported lipid bilayers were formed by vesicle fusion on a hydrophilic glass coverslip that had been cleaned as described previously (32). The t-SNARE vesicles were added at a total lipid concentration of 25 μM. After deposition of t-SNARE vesicles at 4°C for 2.5 h, the bilayers were warmed to 37°C for 1–2.5 h and gently washed three times with buffer (60 cell volumes total) just before docking and fusion studies were performed. These conditions produced a high percentage of fast fusion events and homogeneous diffusion of lipid labels after fusion. Docking and fusion measurements were obtained at room temperature (typically 25°C). In two earlier studies (31,32), we erroneously reported the temperature during docking and fusion measurements as 37°C, when in fact it was 25°C.

Total internal reflection fluorescence microscopy

Details of the total internal reflection fluorescence (TIRF) technique used, including laser intensities and filter sets, are given in the Supporting Material. Briefly, laser beams at 488 nm (calcein excitation) and (depending on the lipid labels) either 514 nm (TRITC-DHPE excitation) or 561 nm (R18/Texas Red-DHPE excitation) illuminated the sample in TIR mode. Fluorescence from calcein and the lipid label were separated by a dichroic mirror and imaged side by side on an EMCCD camera (''two-channel movies''). Movies at 5 ms/frame or, occasionally, 1 ms/frame were recorded by a fast EMCCD camera with 24 μm $\times$ 24 μm pixels (DV860ECS-BV; Andor Technologies, Belfast, Northern Ireland), corresponding to 240 nm $\times$ 240 nm at the sample. We also acquired one-channel movies in which only the lipid label and its corresponding excitation laser were present. These 40 ms/frame movies were recorded by an EMCCD camera with 16 μm $\times$ 16 μm pixels (DV887ECS-UVB; Andor Technologies), equivalent to 160 nm $\times$ 160 nm at the sample. A circular area with diameter ~40 μm was illuminated with a total laser intensity of 60 μW at 514 nm (TRITC-DHPE) or 561 nm (R18 or Texas Red-DHPE).

Fusion assay

After the bilayer deposition was completed, the membranes were rinsed with 2 mL of warm buffer to remove unfused vesicles. They were then removed from a 37°C incubator and placed on the stage, after which the cells dropped to room temperature within seconds. Before addition above the lipid bilayer, v-SNARE vesicles were chilled on ice, which seems essential for fast fusion. We flowed 200 μL of cold v-SNARE vesicle solution through the cells, fully exchanging the solution in ~2 s. Movies began 10–20 s later, after the microscope was manually focused.

Fluorescence intensity measurements were performed in MetaMorph (Molecular Devices, Sunnyvale, CA). For 40 ms/frame movies, a circular region with a radius of 0.8 μm was manually drawn around each of the fusing vesicles. MetaMorph summed the fluorescence intensity from all of the pixels within the region to generate a plot of integrated fluorescence intensity versus time, which we call $I_{0.8\ \mu m}(t)$. For 5 ms/frame and 1 ms/frame movies, the region of integration has a radius 1.2 μm, so the intensity traces are called $I_{1.2\ \mu m}(t)$.

RESULTS

Hemifusion events in one-color movies

Our previous study (31) of SNARE-driven hemifusion used TRITC-DHPE labels in the v-SNARE vesicles. Hemifusion events were observed as partial release of labeled lipids in an outgoing radial wave, leaving behind a bright core that subsequently did or did not fuse (productive versus dead-end hemifusion events). Fig. S1 in the Supporting Material shows examples of the time dependence of integrated fluorescence intensity within a circle of 0.8-μm radius at 40 ms/frame. The three lipid labels used in this work (1% TRITC-DHPE, 5% R18, and 5% Texas Red-DHPE) are compared there. With TRITC-DHPE and Texas Red-DHPE labeling, hemifusion events (as judged by the persistent bright core left behind after the first wave of labels diffused away) often showed a second dequenching burst of fluorescence at the moment when the core also fused. With R18 labeling, the second burst was seldom observed. The reason is flip-flop from the inner to the outer leaflet on the timescale of the core fusion event, as explained below.

Two-color, 5 ms movies reveal three types of fusion events

We obtained two-color, 5 ms/frame movies of single vesicles docking and fusing, using the green-emitting calcein to label content and the red-emitting R18 to label lipids. We identified three types of fusion events based on the relative sequence of content release and lipid mixing: 1), prompt, full fusion (type 1), meaning that all lipids mix and the content is released essentially simultaneously within 5–10 ms at time t_{fus} (Fig. 1 *a*); 2), productive hemifusion (type 2), in which the outer leaflet mixes at time t_{hemi}, after which the inner leaflet mixes and content is released after the additional time interval t_{core} (Fig. 1 *b*); and 3), dead-end hemifusion (type 3), in which the outer leaflet mixes at t_{hemi} but the content is never released on the 10 s timescale of the movie (Fig. 1 *c*). Justification of these interpretations follows.

Relative timing of R18 and calcein signals

The relative timing of the two signals provides detailed information about the nature and sequence of the lipid mixing and content release events that occur during the fusion process. The idealization in Fig. 2 illustrates how we extract timing information from traces of calcein and R18 fluorescence intensity integrated over a circle of 1.2 μm radius. Firm docking causes a sharp step upward of both signals to ''pedestal values''. The first channel in which the R18 signal increases significantly from its pedestal value (labeled frame 0 in Fig. 2) marks the time t_{fus} (for a prompt, full fusion event) or t_{hemi} (for hemifusion events). The R18 signal continues to rise for some 2–20 frames (10–100 ms); only very rarely does it jump directly to the maximum value in one frame. It reaches its peak at a time we call $t_{R18\ rise}$. In Fig. 2, this occurs

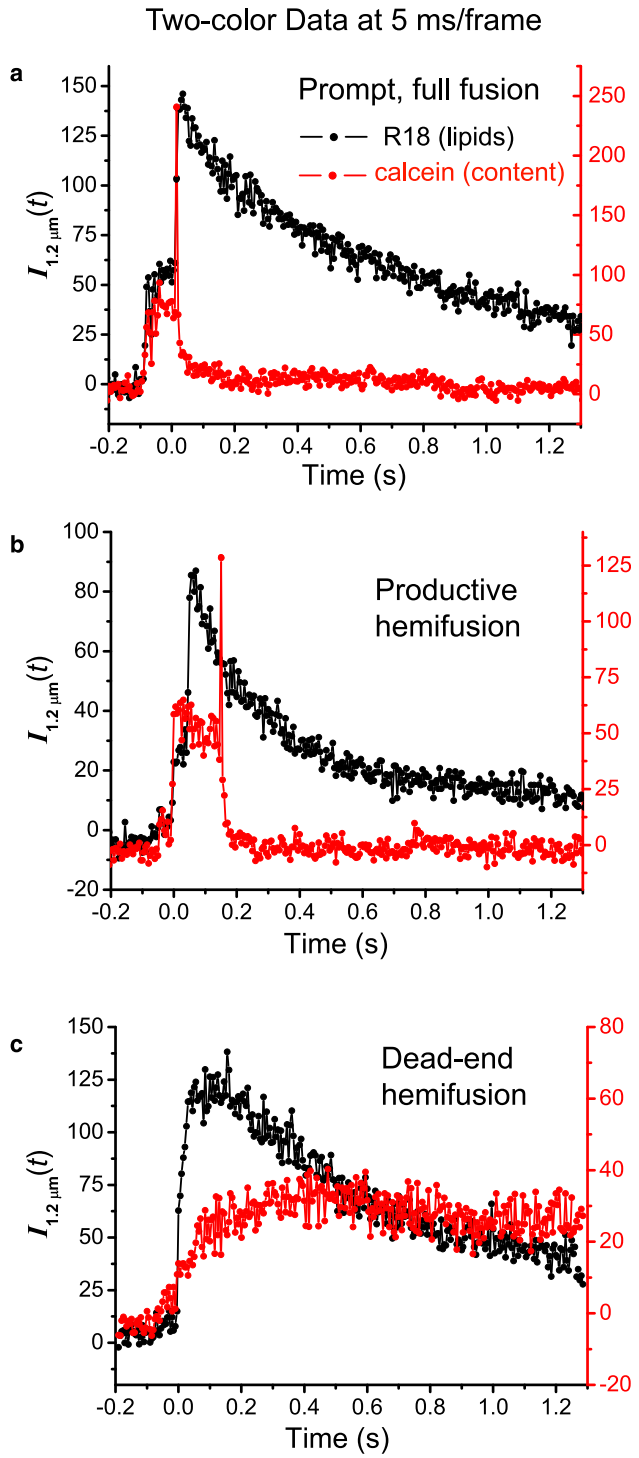

FIGURE 1 Representative examples of fluorescence intensity traces $I_{1.2\mu m}(t)$ (intensity integrated over a 1.2 μm radius circle) for three types of events from two-color, 5 ms/frame movies: (*a*) prompt, full fusion (type 1); (*b*) productive hemifusion (type 2); and (*c*) dead-end hemifusion (type 3). The v-SNARE vesicles are labeled with 5% R18 and 50 mM calcein. Laser illumination area is ~160 μm^2 for both the 488 nm laser (15 μW) and 561 nm laser (10 μW). The v-SNARE vesicle lipid composition is (*a* and *b*) 15% DOPS, 30% DOPE, 5% R18, and 50% POPC; and (*c*) 15% DOPS, 60% DOPE, 5% R18, and 20% POPC.

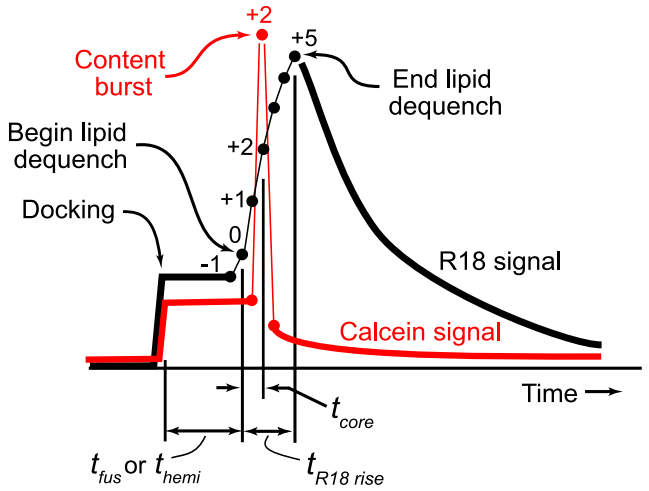

FIGURE 2 Schematic of timing measurements. See text for details.

at frame +5; we would record $t_{\mathrm{R18\ rise}} = 25$ ms. The R18 signal then gradually decays to the baseline with a time dependence that is well fit by the diffusion equation with typical $D_{\mathrm{R18}} \approx 1\ \mu\mathrm{m}^2\text{-s}^{-1}$ (Fig. S2). In contrast, the calcein burst always occurs in exactly one 5 ms frame, after which the content signal drops almost to the baseline value. This surprising time dependence is analyzed in detail below. We measure t_{core} as the time between the beginning of lipid dequenching (frame 0) and the calcein burst; in Fig. 2, this occurs at frame +2, so that $t_{\mathrm{core}} = 10$ ms.

We cannot control the timing of events relative to the sequence of camera frames. Evidently, content release and dequenching is a kinetically faster process than mixing of R18 molecules with the planar bilayer. We estimate the timescale of calcein release and dequenching to be $\leq$2 ms; if it were longer, the burst intensity would sometimes remain high for two frames. The timescale of R18 mixing with the planar bilayer is evidently $\geq$5 ms; if were shorter, we would more often see the signal rise in one frame. As discussed below, for events with $t_{\mathrm{R18\ rise}}$ of ~10 ms or less, the rise time may be limited by the timescale of diffusion on the surface of the vesicle to ''find'' the small zone connecting the leaflet(s) of the vesicle to the leaflet(s) of the bilayer. When the rise time is much longer, this suggests some sort of barrier or bottleneck for lipid mixing.

Prompt, full fusion events (type 1) and fast, productive hemifusion events (type 2) are distinguished by the time t_{core}. The R18 signal takes two or more frames to reach its peak; the single-frame calcein burst may occur at frame 0 (the first detectable increase of R18 signal), in which case $t_{\mathrm{core}} = 0$; or at frame 1, 2, etc. (for which $t_{\mathrm{core}} = 5$ ms, 10 ms, etc.). In practice, we classify all events with $t_{\mathrm{core}} \leq 5$ ms as prompt, full fusion events (type 1). Events with $t_{\mathrm{core}} \geq 10$ ms are classified as hemifusion events (productive, type 2, if the content is eventually released during the 10 s movie, or dead-end, type 3, if it is never released during the movie). The $t_{\mathrm{core}} = 5$ ms events are ambiguous; we include them as type 1 to allow for a one-channel error in determining the beginning of the rise in the noisy R18 signal. For a very few events, we obtain $t_{\mathrm{core}} = -5$ ms; this presumably indicates that full fusion occurred late in a camera frame, so that the calcein burst registers in the frame just before we first sense the R18 rise.

In most type 2 events, the R18 signal shows neither a second ''burst'' of fluorescence nor a persistent core of R18 fluorescence that remains after the first wave has diffused away. As shown below, the second burst is missing due to fast flip-flop of R18. How then can we be certain that the calcein burst faithfully signals the onset of inner-leaflet mixing? The best evidence comes from dual labeling experiments using Texas Red-DHPE (which does not flip-flop on the relevant timescale) and calcein, as described below.

Evidence for R18 flip-flop and FRET from calcein to inner-leaflet R18

Two effects combine to prevent observation of a second burst of R18 fluorescence dequenching that would signal core (inner-leaflet) fusion. When core fusion occurs within ~200 ms of hemifusion, the R18 signal increase is obscured by the lingering diffuse distribution of outer-leaflet labels, which typically requires ~500 ms to decay by a factor of 2 (Fig. S2). The same problem masked relatively fast core fusion events in the original study using TRITC-DHPE labels (31). In addition, at the instant of hemifusion, lipids and lipid markers in the outer leaflet of the vesicle mix with lipids in the planar t-SNARE bilayer on a timescale of ~5–20 ms and the outer-leaflet markers begin to diffuse away. This causes a gradient in lipid marker concentration between the inner and outer leaflets, enabling net flip-flop of labels to the outer leaflet. For R18 in the 60% DOPE vesicles, we estimate below that the timescale for flip-flop is ~200 ms. When core fusion occurs significantly more slowly than R18 flip-flop, on a timescale of $\geq$200 ms, the inner-leaflet labels transfer to the outer leaflet, mix with the planar bilayer, and escape the observation zone before the core fusion event that would have caused abrupt, observable dequenching. Again, no second burst of intensity is observed.

We cannot observe R18 flip-flop directly, but we can infer its timescale from type 3 events (dead-end hemifusion) labeled with both calcein and R18 (Fig. 1 *c*). In such events, the calcein remains trapped within an intact vesicle until the end of movie. For all such events, the calcein signal typically increases slowly, by about a factor of 2, beginning at the time t_{hemi}. We believe this is due to gradual relief of quenching of calcein intensity caused by fluorescence resonance energy transfer (FRET) to nearby inner-leaflet R18 labels. The ~200 ms timescale of the rise in calcein signal for type 3 events is consistent with both a direct measurement (39) and an indirect estimate (40) of the R18 flip-flop timescale in the literature. The detailed evidence for FRET from

calcein to R18 is given in the Supporting Material, including Fig. S4.

Texas Red-DHPE confirms coincidence of content release with core fusion

To further test the assumption that the calcein dequenching event is an accurate marker of t_{core}, we carried out analogous imaging experiments substituting Texas-Red-DHPE for R18 as the lipid label. Texas Red-DHPE is a double-tailed, phospholipid-based label with similar spectral properties to R18, but evidently with a much slower flip-flop rate. Accordingly, with 5% Texas Red-DHPE labels in 40 ms/frame one-color movies, productive hemifusion events (type 2) show two bursts of intensity (Fig. S1 *c*), arising from the successive fusion of the outer leaflet and the inner leaflet of the v-SNARE vesicle. This is the same behavior observed in one-color movies using TRITC-DHPE labels (Fig. S1 *a*). In type 2 events imaged at 5 ms/frame using both Texas Red-DHPE and calcein (Fig. S3 *b*), the sharp calcein signal burst from content release is always coincident with the second peak in the lipid channel to within 10 ms (all 12 events observed). The content is released from the vesicle at the same time as core lipid fusion to within the time resolution of the measurements.

In dead-end hemifusion events (type 3) using Texas Red-DHPE as the lipid label, there is a single peak in the lipid channel due to hemifusion. Subsequently, the lipid core and calcein remain punctal for the remainder of the movie. Rather than increasing in intensity after hemifusion due to relief of FRET by lipid flip-flop, the calcein intensity slowly decreases. FRET should also occur from calcein to Texas Red, but evidently Texas Red-DHPE in the inner leaflet does *not* flip-flop to the outer leaflet on the timescale of interest after hemifusion. The quenching efficiency remains constant in time. We attribute the decrease in calcein intensity to gradual photobleaching of the content (Fig. S3 *c*) on a ~1 s timescale. Photobleaching is presumably also occurring in the R18 labeling case, but relief of FRET dominates and causes the net increase in content intensity for dead-end events. The different trends of calcein intensity change after hemifusion for R18 and Texas-Red-DHPE as the lipid labels again indicate that the calcein intensity increase after hemifusion for the R18-labeled vesicle is due to R18 flip-flop rather than leaking of calcein content.

In summary, all of the evidence is consistent with our assertion that the sharp rise in calcein intensity accurately marks the onset of core (inner-leaflet) fusion with the planar bilayer even when the R18 channel shows no evidence of a second wave of lipid mixing. The typical timescale of core fusion in type 2 events is similar (10–400 ms) using the R18 and the Texas Red labels. However, the Texas Red-DHPE label decreases the overall frequency of hemifusion events (Table S1). The positive curvature due to the large Texas Red headgroup may be accelerating core fusion in comparison with TRITC or R18 labels.

3D content release by "bursting" of the vesicle as core lipids fuse

We expected that calcein would be deposited in the 1–3 nm thick layer of water between the lower leaflet of the bilayer and the surface of the glass substrate (41,42), after which it would dequench and undergo essentially two-dimensional (2D) diffusion out of the observation zone. However, the calcein dequenching burst is only one frame wide ($\leq$5 ms duration). It is in fact very difficult to observe these bursts in 40 ms/frame movies. This caused us to examine the possibility that calcein is in fact released into the 3D space above the bilayer and escapes the observation zone by fast, 3D diffusion in buffer. 3D escape would presumably be much faster than 2D escape due to the larger calcein diffusion coefficient in buffer versus the thin water layer, and also because the evanescent field intensity in TIRF microscopy penetrates the space above glass with a characteristic length of only ~100 nm. To distinguish 3D from 2D diffusion, we obtained two-color, 1 ms/frame movies by increasing the laser intensity. One example of the decay of integrated calcein intensity within a circle of 1.2 μm radius is shown in Fig. 3 *a*. Comparisons with the 2D and 3D diffusion models follow.

2D and 3D theoretical intensity decay models

TIRF measurements of the relative fluorescence quantum yield ϕ_{rel} for calcein concentrations up to 75 mM calcein are shown in Fig. 3 *b*. The relative quantum yields obtained from TIRF measurements are much higher than the apparent results from a conventional cuvette and fluorimeter. Taking ϕ_{rel} (100 μM) to be 1, then ϕ_{rel} (1 mM) = 0.85 using TIRF (Fig. 3 *b*), which is more than 1000-fold higher than the incorrect result of 5.9×10^{-4} obtained from a 1-cm cuvette with a standard fluorimeter (Fig. 3 *b*). With ϕ_{rel} defined as one in dilute solution, the self-quenching data from TIRF fit an exponential decay:

$$\phi_{rel} = \exp(-59.3 \times [\text{calcein}]), \quad (1)$$

Here [calcein] is measured in molar units. To test for possible contributions from calcein molecules bound to the glass surface, we repeated the TIRF measurements by adding calcein above a planar lipid bilayer. The results are identical (Fig. 3 *b*), indicating that we are measuring self-quenching in solution phase calcein.

Using ϕ_{rel} from Eq. 1, we built 2D and 3D time-dependent diffusion models for the escape of calcein from the observation zone and the corresponding time-dependence of the integrated fluorescence intensity. Details are given in the Supporting Material. Both models take into account the number of molecules within the observation region, dequenching of calcein molecules as [calcein] decreases in time, and (for the 3D case) the exponential decay of the evanescent wave intensity. For comparison with the 1 ms/frame data (Fig. 3 *a*), we calculated the integrated fluorescence intensities from

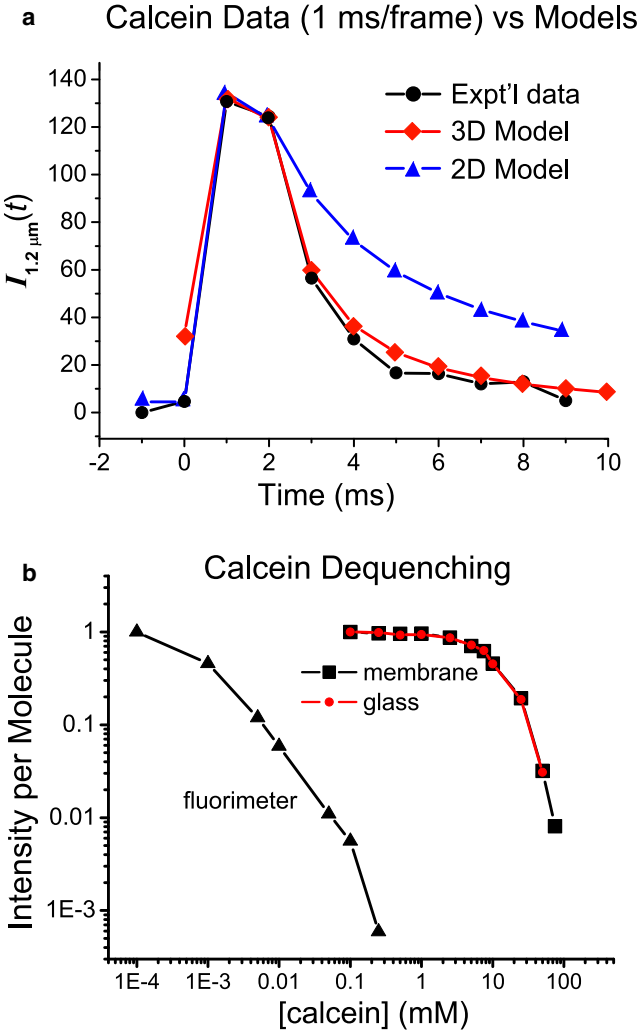

FIGURE 3 (*a*) Comparison of integrated calcein fluorescence intensity trace $I_{1.2\mu m}(t)$ from 1 ms, two-color movies with 3D and 2D diffusion model calculations using $D_{calcein} = 200\ \mu m^2/s$ in both cases. See text and the Supporting Material for details. (*b*) Relative intensity per calcein molecule versus [calcein] from fluorimeter and TIRF measurements. The TIRF measurements were the same on hydrophilic glass (*circles*) and hydrophilic glass covered by a supported lipid bilayer of 2% DOPS and 98% POPC (*squares*). See text for details.

0 to 55 ms in 50 μs time intervals, and averaged the values over 20 time intervals to match the 1 ms camera exposure time. We assume 50 mM initial calcein concentration, and 200 μm^2-s^{-1} diffusion coefficient for both 2D and 3D diffusion models.

A comparison of the model results with the experimental calcein intensity decay traces (Fig. 3 *a*) shows that the 3D model matches the data very well, whereas the 2D model decays much more slowly than the data. To examine the effect of different initial calcein concentrations, we tried values from 10 mM to 200 mM. In all cases, the 2D model intensity decayed much too slowly. In addition, 200 μm^2-s^{-1} is almost surely an overestimate of the diffusion coefficient of calcein in the 1–3 nm thick aqueous layer between the glass surface and the lower leaflet of the bilayer. The region is only several water molecules thick, comparable to twice the long dimension of a calcein molecule. Furthermore, the water molecules are not like bulk water; presumably, they are strongly oriented by transient binding to the bilayer and the charged, hydrophilic glass surface.

We cannot reconcile the prompt burst of calcein fluorescence with 2D diffusion in the thin water layer, and the 3D bursting model fits the data very well. Thus we conclude that immediately upon fusion of the inner-leaflet lipids of the v-SNARE vesicle with the planar bilayer, the vesicle bilayer ruptures and quickly emits all the calcein content into 3D space above the planar bilayer. Such rupture may be due to increased pressure within the vesicle as it fuses and flattens, as discussed below.

Tests for effect of laser intensity on fusion kinetics

Bowen and co-workers (33) found that SNARE-dependent fusion of proteoliposomes onto a planar lipid bilayer on a 10 s timescale was driven primarily by the temperature rise due to laser heating of the self-quenched calcein content at 200 mM. We therefore checked for a dependence of fusion kinetics on laser intensities, but found none (details in Supporting Material text and Fig. S5). In our study there was four times less calcein content and the vesicles fused much more rapidly; thus, there was little time in which the 488-nm laser could heat the vesicle.

Ensemble kinetics of full fusion, hemifusion, and core fusion

Using the new methodology to measure ~600 events from 5 ms/frame, two-color movies (calcein and R18), we assembled experimental histograms of t_{fus} (for type 1 events), t_{hemi} (type 2 and type 3 events), and t_{core} (type 2 events) as shown in Fig. S7. The v-SNARE vesicles contained 0%, 30%, or 60% DOPE as indicated. The data were binned in 10 ms intervals in Fig. 4 to improve the signal/noise ratio and then fit to a single exponential decay, yielding an approximate rate constant for each individual step ($k_{fus} = \tau_{fus}^{-1}$, $k_{hemi} = \tau_{hemi}^{-1}$, or $k_{core} = \tau_{core}^{-1}$). The fits are reasonably good; however, sometimes there is evidence of a more slowly decaying tail of the distribution. The fits do not attempt to account for the variable phase between camera frames and events.

Table 1 summarizes best-fit rate constants and the measured branching fractions into each outcome. Both prompt, full fusion events and hemifusion events occur with a time constant of ~5–10 ms, essentially independently of the DOPE percentage in the v-SNARE vesicle. The branching fraction f_{hemi} for productive and dead-end hemifusion events combined rises sharply from 5% to 14% to 61% as the DOPE percentage increases from 0% to 30% to 60%. Our initial study at 0% DOPE in the v-SNARE vesicles (32) used a much noisier intensified camera. The study presented here reveals a threefold faster rate constant for k_{fus} at 0%

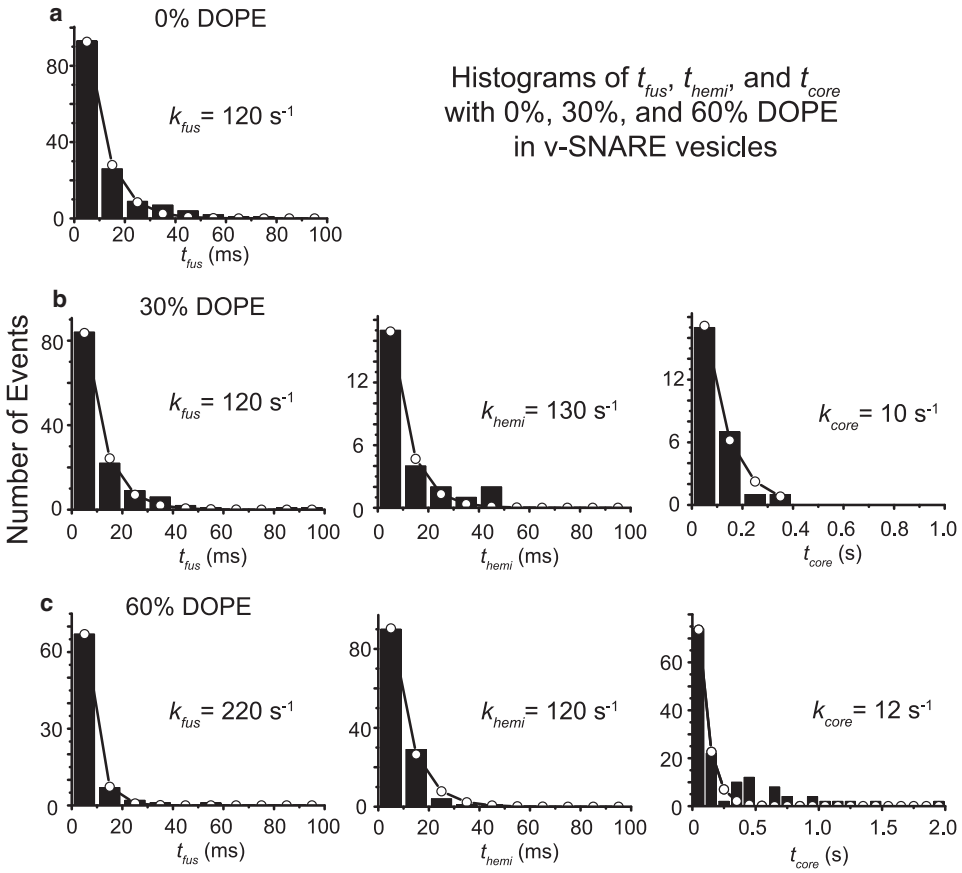

FIGURE 4 Histograms of t_{fus}, t_{hemi}, and t_{core} for v-SNARE vesicles with (*a*) no DOPE, (*b*) 30% DOPE, and (*c*) 60% DOPE from two-color, 5 ms/frame movies. Data were binned into 10 ms intervals before fitting to a single-exponential function (*open circles*) with time constant as shown. Some of the histograms show evidence of a long-time tail, suggesting heterogeneity in the kinetics. See Table 1 for best-fit rates and branching fractions, and Fig. S5 for histograms binned into 5 ms intervals.

DOPE. Both studies used 5 ms camera frames, but we believe the current results to be much more accurate. First, the higher signal/noise ratio from the EMCCD camera used in this study allows us to detect firm docking of the vesicle and the rise in lipid signal much more sensitively. This tends to move the choice of the docking frame to a later time because we observe vesicle motion more clearly. Second, the improved signal/noise ratio also tends to move the choice of the initial rise in R18 signal to an earlier time because the pedestal intensity of a docked vesicle is smoother. Both of these effects shorten measurements of t_{fus} (or t_{hemi}) and also make the measurement more accurate.

In comparison with a subsequent study of the effects of DOPE on hemifusion using only the lipid label TRITC-DHPE (31), we now obtain 10 times faster k_{hemi} and much larger branching into hemifusion events at the same 60% DOPE content in the v-SNARE vesicles. The faster k_{hemi} is due in part to the same effects of a higher signal/noise ratio, but primarily to the reclassification of many fast events from prompt, full fusion to productive hemifusion due to sensitive detection of the calcein burst. Similarly, the 20-fold increase in k_{core} at 60% DOPE is again due primarily to the same reclassification of events having $t_{\text{core}} \sim 100$ ms.

TABLE 1 Fusion and hemifusion rate constants and branching fractions from 5 ms/frame movies using dual labeling with R18 and calcein

		Full fusion‡		Hemifusion‡				
v-SNARE vesicle % DOPE*	N_{total}†	f_{fus}	k_{fus} (s^{-1})	f_{hemi}	k_{hemi} (s^{-1})	f_{core}	k_{core} (s^{-1})	$f_{\text{dead-end}}$
0	172	0.95	120 ± 30	0.05	–	–	–	–
30	219	0.82	120 ± 30	0.18	130 ± 30	0.18	10.2 ± 2.5	–
60	200	0.35	220 ± 80	0.65	120 ± 30	0.39	11.8 ± 3.0	0.26

*In addition to DOPE, vesicles contain 5% R18 labels, 15% DOPS, and the remainder POPC.
†Total number of events measured.
‡See text for classification scheme. Branching fractions are f_{fus} for prompt, full fusion, and f_{hemi} for the sum of productive (f_{core}) and dead-end ($f_{\text{dead-end}}$) hemifusion. The rate constant k_{hemi} includes both productive and dead-end hemifusion events; in the former, k_{core} measures the rate at which hemifusion intermediates decay via core fusion.

DISCUSSION

In both of our previous studies of single-vesicle fusion (32) and hemifusion (31), we tested the effect of omitting SNAP-25 to form a syx-only bilayer supported on glass. There was no clearly discernible effect on either the branching between full fusion and hemifusion or the timescale of full fusion and hemifusion events. We did not retest for dependence on SNAP-25 in the work presented here because the materials are the same and our new results are consistent with the old. The only change is the presence of 50 mM calcein inside the v-SNARE vesicles, and the fusion/hemifusion kinetics and branching are the same with and without 50 mM calcein (Table S1). This strongly indicates that the current results would not change appreciably in the absence of SNAP-25. It seems that formation of ''promiscuous'' SNARE complexes leads to fast fusion or hemifusion in this low-barrier assay.

The speed and sensitivity of EMCCD cameras enable the study of single-vesicle docking, prompt full fusion, hemifusion, and core fusion with a time resolution of 5 ms/frame, or even 1 ms/frame. The dual-labeling experiments using Texas Red-DHPE and calcein demonstrate that the sharp increase in calcein signal faithfully reports on inner-leaflet lipid mixing. This allows us to properly identify productive hemifusion events on a 10–200 ms timescale that previously went undetected using lipid markers alone. On that timescale, the second intensity burst of TRITC-DHPE or R18 labels is difficult to observe on the background of fluorescence from outer-leaflet labels before they diffuse away. R18 inner leaflet labels have the further disadvantage of flip-flopping and dequenching slowly so as not to produce a strong second burst.

Our main conclusion is that hemifusion occurs more frequently and much more rapidly in this in vitro SNARE-induced fusion assay than previously reported, particularly with 60% DOPE in the v-SNARE vesicles (Table 1). The new 5 ms data reveal many fast, productive hemifusion events that were previously classified as prompt, full fusion events in the original 40-ms data using only TRITC-DHPE labels. In addition, it is now clear that prompt, full fusion and hemifusion occur on essentially the same timescale, with $\tau_{fus} = k_{fus}{}^{-1}$ and $\tau_{hemi} = k_{hemi}{}^{-1}$ of ~5–10 ms, regardless of DOPE content (Table 1). In our earlier study, we incorrectly concluded that the outer-leaflet mixing in hemifusion events occurred substantially more slowly than prompt, full fusion events. As before, the branching fraction into hemifusion versus full fusion increases markedly with increasing %DOPE.

Of interest, the R18 dequenching/reorientation events characterized by $t_{R18\ rise}$ usually occur more slowly than the 5-ms camera frame time (Fig. S8). We may well be approaching a fundamental timing limit on the measurement of fast fusion events using dequenching of lipid-based labels. Assuming that the kinetics of rhodamine dimer dissociation is faster than the low-millisecond timescale of interest, the limit is probably set by the timescale of diffusion of labels within the vesicle bilayer to find the small area or seam where lipids from the vesicle and planar bilayer exchange. This is discussed further in the Supporting Material.

The prompt calcein intensity bursts, which occur in ≤ 5 ms, are very useful for marking the instant of inner-leaflet mixing. However, it is disappointing that the content is evidently released abruptly into the 3D space above the planar bilayer rather than into the ~2 nm thin, watery space between the glass and the planar bilayer. In hindsight, this is perhaps not too surprising. The space is only several water layers thick, and we expect strong interaction of these few water molecules with the polar head region of the bilayer and with the charged $=SiO^-$ and polar $=SiOH$ groups of the hydrophilic glass surface.

A possible physical picture of the bursting event can be described as follows: As the lipids of the vesicle core and planar bilayer begin to mix, the potential energy stored in the 50-nm-diameter vesicle as curvature strain provides a driving force for flattening of the vesicle. Flattening decreases the volume within the vesicle, which builds internal pressure. Evidently the pressure builds sufficiently rapidly to rupture the vesicle-bilayer structure, possibly at the ''seam'' where SNARE proteins act (see below). The calcein is essentially always released in a single burst; only a very few ''double-bursting'' events are observed. Evidently the rupture seldom reseals. It remains unclear whether a proper fusion pore connecting the vesicle internal volume with the thin water space ever develops. If a fusion pore does open, the flow conductance through the thin space must be insufficient to relieve the pressure buildup within the flattening vesicle quickly enough, and bursting occurs to relieve this pressure.

Such bursting behavior may be related to other observations suggesting that a variety of ''fusases'' (proteins that induce fusion of two bilayers, such as hemagglutinin in viruses or ternary SNARE complexes in neurons) cause content leakage on the same timescale as fusion, both in vivo and in vitro (37). Examples include yeast vacuole fusion (43), lysis of mutated yeast mating pairs (44,45), and fusion of viruses to synthetic liposomes (46–48). These results lend support to an asymmetric model of membrane fusion based on coarse-grained simulations (49,50) in which formation of a stalk intermediate promotes formation of adjacent holes in one or both bilayers. Subsequently, the holes may either expand, leading to lysis, or be enveloped by the stalk, leading to fusion. The branching betweeen lysis and fusion may in turn be determined by the degree of organization of the SNARE complexes in space (37). In this view, our fast fusion assay may lead to bursting due to its lack of control over SNARE organization, which may require different lipids or additional proteins.

Our results serve as a reminder that measurement of content-mixing signals remains important. The few studies that have examined the relatively slow case of SNARE-

induced vesicle-vesicle fusion have shown variable outcomes. A recent study found content mixing on the same timescale as fusion (3). A study based on duplex formation between oligonucleotides separately reconstituted into v-SNARE and t-SNARE vesicles also found that fusion of the lipids occurs on the same timescale as mixing of content, without significant leakage (51). In another study, investigators used polyethylene glycol to accelerate fusion events by aggregating vesicles, and found that lipid mixing was accompanied by a significant amount of content leakage (52). Yet another group showed that content slowly leaked from vesicles regardless of whether they were mixed together or kept as separate populations, but the presence of the content label prevented SNARE complexes from forming (53).

To our knowledge, the only other content-release study involving a SNARE-driven, single-vesicle fusion assay is that of Bowen and co-workers (33). In a vesicle-plus-supported bilayer geometry like our own, they used labeled synaptobrevin to monitor v-SNARE vesicle docking, and calcein to signal content release and thus fusion. Although many docking events led to apparent fusion, a few led to sudden content bursting much as observed here. All such events occurred on a ~10 s kinetic timescale after the probe laser was turned on, and were thermally driven by laser heating of the vesicle via calcein absorption. Our fusion and hemifusion kinetics are ~1000 times faster, for reasons that remain unclear. We found no evidence of laser heating (Fig. S5), perhaps because our vesicles fuse in ~10 ms, which is too short a time to permit a significant temperature rise. Both assays share the property that removal of SNAP-25 from the t-SNARE vesicles used to make the supported bilayer has no obvious effect on v-SNARE vesicle docking and fusion behavior.

Clearly, an important next step in development of the vesicle-plus-planar bilayer assay is to increase the height of the space available for proper content release to test for formation of a fusion pore. This might be done by interposing a layer of a hydrophilic polymer spacer between the glass and the t-SNARE bilayer (54). An alternative is to use giant unilamellar vesicles to mimic the planar bilayer (55). In yet another approach, Yoon and co-workers (36) studied single vesicle-plus-vesicle docking and fusion events by tethering one vesicle type to a passivated glass surface. If we can achieve content release into the proper space, studies of the time sequence of content release versus lipid mixing with 1–5 ms resolution may provide new insight into the structure of the fusion pore (5).

SUPPORTING MATERIAL

Additional text, equations, a table, references, and figures are available at http://www.biophysj.org/biophysj/supplemental/S0006-3495(09)00658-4.

We thank the members of the Chapman laboratory for many helpful discussions and for the use of facilities for purification of SNARE proteins and proteoliposomes.

We also thank the National Institute of Neurological Disorders and Stroke for funding this work under grant 5R01NS051518.

REFERENCES

1. Jahn, R. 2008. Some classic papers in the field of membrane fusion–a personal view. *Nat. Struct. Mol. Biol.* 15:655–657.
2. Chapman, E. R. 2008. How does synaptotagmin trigger neurotransmitter release? *Annu. Rev. Biochem.* 77:615–641.
3. Kreye, S., J. Malsam, and T. H. Sollner. 2008. In vitro assays to measure SNARE-mediated vesicle fusion. *Methods Mol. Biol.* 440:37–50.
4. Malinin, V. S., P. Frederik, and B. R. Lentz. 2002. Osmotic and curvature stress affect PEG-induced fusion of lipid vesicles but not mixing of their lipids. *Biophys. J.* 82:2090–2100.
5. Jackson, M. B., and E. R. Chapman. 2006. Fusion pores and fusion machines in Ca^{2+}-triggered exocytosis. *Annu. Rev. Biophys. Biomol. Struct.* 35:135–160.
6. Jahn, R. 2004. Principles of exocytosis and membrane fusion. *Ann. N. Y. Acad. Sci.* 1014:170–178.
7. Sudhof, T. C. 2004. The synaptic vesicle cycle. *Annu. Rev. Neurosci.* 27:509–547.
8. Jahn, R., T. Lang, and T. C. Sudhof. 2003. Membrane fusion. *Cell.* 112:519–533.
9. Wolfel, M., and R. Schneggenburger. 2003. Presynaptic capacitance measurements and Ca^{2+} uncaging reveal submillisecond exocytosis kinetics and characterize the Ca^{2+} sensitivity of vesicle pool depletion at a fast CNS synapse. *J. Neurosci.* 23:7059–7068.
10. Brunger, A. T. 2001. Structure of proteins involved in synaptic vesicle fusion in neurons. *Annu. Rev. Biophys. Biomol. Struct.* 30:157–171.
11. Sutton, R. B., D. Fasshauer, R. Jahn, and A. T. Brunger. 1998. Crystal structure of a SNARE complex involved in synaptic exocytosis at 2.4 A resolution. *Nature.* 395:347–353.
12. Weber, T., B. V. Zemelman, J. A. McNew, B. Westermann, M. Gmachl, et al. 1998. SNAREpins: minimal machinery for membrane fusion. *Cell.* 92:759–772.
13. Rothman, J. E., and G. Warren. 1994. Implications of the SNARE hypothesis for intracellular membrane topology and dynamics. *Curr. Biol.* 4:220–233.
14. Lang, T., and R. Jahn. 2008. Core proteins of the secretory machinery. *Handb. Exp. Pharmacol.* 184:107–127.
15. Jackson, M. B. 2007. In search of the fusion pore of exocytosis. *Biophys. Chem.* 126:201–208.
16. Holt, M., D. Riedel, A. Stein, C. Schuette, and R. Jahn. 2008. Synaptic vesicles are constitutively active fusion machines that function independently of Ca^{2+}. *Curr. Biol.* 18:715–722.
17. Lee, J., and B. R. Lentz. 1997. Evolution of lipidic structures during model membrane fusion and the relation of this process to cell membrane fusion. *Biochemistry.* 36:6251–6259.
18. Lentz, B. R. 1994. Polymer-induced membrane fusion: potential mechanism and relation to cell fusion events. *Chem. Phys. Lipids.* 73:91–106.
19. Burgess, S. W., and B. R. Lentz. 1993. Fluorescence lifetime measurements to monitor membrane lipid mixing. *Methods Enzymol.* 220:42–50.
20. Zimmerberg, J., S. S. Vogel, and L. V. Chernomordik. 1993. Mechanisms of membrane fusion. *Annu. Rev. Biophys. Biomol. Struct.* 22:433–466.
21. Cohen, F. S., M. H. Akabas, J. Zimmerberg, and A. Finkelstein. 1984. Parameters affecting the fusion of unilamellar phospholipid vesicles with planar bilayer membranes. *J. Cell Biol.* 98:1054–1062.
22. Zimmerberg, J., F. S. Cohen, and A. Finkelstein. 1980. Micromolar Ca^{2+} stimulates fusion of lipid vesicles with planar bilayers containing a calcium-binding protein. *Science.* 210:906–908.
23. Cohen, F. S., J. Zimmerberg, and A. Finkelstein. 1980. Fusion of phospholipid vesicles with planar phospholipid bilayer membranes. II. Incorporation of a vesicular membrane marker into the planar membrane. *J. Gen. Physiol.* 75:251–270.
24. Zimmerberg, J., F. S. Cohen, and A. Finkelstein. 1980. Fusion of phospholipid vesicles with planar phospholipid bilayer membranes. I.

Discharge of vesicular contents across the planar membrane. *J. Gen. Physiol.* 75:241–250.

25. Niles, W. D., and F. S. Cohen. 1987. Video fluorescence microscopy studies of phospholipid vesicle fusion with a planar phospholipid membrane—nature of membrane-membrane interactions and detection of release of contents. *J. Gen. Physiol.* 90:703–735.
26. Woodbury, D. J., and J. E. Hall. 1988. Vesicle-membrane fusion—observation of simultaneous membrane incorporation and content release. *Biophys. J.* 54:345–349.
27. Chanturiya, A., L. V. Chernomordik, and J. Zimmerberg. 1997. Flickering fusion pores comparable with initial exocytotic pores occur in protein-free phospholipid bilayers. *Proc. Natl. Acad. Sci. USA.* 94:14423–14428.
28. Jahn, R., and T. C. Sudhof. 1999. Membrane fusion and exocytosis. *Annu. Rev. Biochem.* 68:863–911.
29. Tucker, W. C., T. Weber, and E. R. Chapman. 2004. Reconstitution of Ca^{2+}-regulated membrane fusion by synaptotagmin and SNAREs. *Science.* 304:435–438.
30. Chicka, M. C., E. F. Hui, H. S. Liu, and E. R. Chapman. 2008. Synaptotagmin arrests the SNARE complex before triggering fast, efficient membrane fusion in response to Ca^{2+}. *Nat. Struct. Mol. Biol.* 15:827–835.
31. Liu, T., T. Wang, E. R. Chapman, and J. C. Weisshaar. 2008. Productive hemifusion intermediates in fast vesicle fusion driven by neuronal SNAREs. *Biophys. J.* 94:1303–1314.
32. Liu, T. T., W. C. Tucker, A. Bhalla, E. R. Chapman, and J. C. Weisshaar. 2005. SNARE-driven, 25-millisecond vesicle fusion in vitro. *Biophys. J.* 89:2458–2472.
33. Bowen, M. E., K. Weninger, A. T. Brunger, and S. Chu. 2004. Single molecule observation of liposome-bilayer fusion thermally induced by soluble N-ethyl maleimide sensitive-factor attachment protein receptors (SNAREs). *Biophys. J.* 87:3569–3584.
34. Fix, M., T. J. Melia, J. K. Jaiswal, J. Z. Rappoport, D. You, et al. 2004. Imaging single membrane fusion events mediated by SNARE proteins. *Proc. Natl. Acad. Sci. USA.* 101:7311–7316.
35. Yoon, T. Y., X. Lu, J. Diao, S. M. Lee, T. Ha, et al. 2008. Complexin and Ca^{2+} stimulate SNARE-mediated membrane fusion. *Nat. Struct. Mol. Biol.* 15:707–713.
36. Yoon, T. Y., B. Okumus, F. Zhang, Y. K. Shin, and T. Ha. 2006. Multiple intermediates in SNARE-induced membrane fusion. *Proc. Natl. Acad. Sci. USA.* 103:19731–19736.
37. Engel, A., and P. Walter. 2008. Membrane lysis during biological membrane fusion: collateral damage by misregulated fusion machines. *J. Cell Biol.* 183:181–186.
38. Reference deleted in proof.
39. Melikyan, G. B., B. N. Deriy, D. C. Ok, and F. S. Cohen. 1996. Voltage-dependent translocation of R18 and DiI across lipid bilayers leads to fluorescence changes. *Biophys. J.* 71:2680–2691.
40. Wessels, L., M. W. Elting, D. Scimeca, and K. Weninger. 2007. Rapid membrane fusion of individual virus particles with supported lipid bilayers. *Biophys. J.* 93:526–538.
41. Johnson, S. J., T. M. Bayerl, D. C. McDermott, G. W. Adam, A. R. Rennie, et al. 1991. Structure of an adsorbed dimyristoylphosphatidylcholine bilayer measured with specular reflection of neutrons. *Biophys. J.* 59:289–294.
42. Kiessling, V., and L. K. Tamm. 2003. Measuring distances in supported bilayers by fluorescence interference-contrast microscopy: polymer supports and SNARE proteins. *Biophys. J.* 84:408–418.
43. Starai, V. J., C. M. Hickey, and W. Wickner. 2008. HOPS proofreads the trans-SNARE complex for yeast vacuole fusion. *Mol. Biol. Cell.* 19:2500–2508.
44. Aguilar, P. S., A. Engel, and P. Walter. 2007. The plasma membrane proteins Prm1 and Fig1 ascertain fidelity of membrane fusion during yeast mating. *Mol. Biol. Cell.* 18:547–556.
45. Jin, H., C. Carlile, S. Nolan, and E. Grote. 2004. Prm1 prevents contact-dependent lysis of yeast mating pairs. *Eukaryot. Cell.* 3:1664–1673.
46. Blumenthal, R., and S. J. Morris. 1999. The influenza haemagglutinin-induced fusion cascade: effects of target membrane permeability changes. *Mol. Membr. Biol.* 16:43–47.
47. Frolov, V. A., A. Y. Dunina-Barkovskaya, A. V. Samsonov, and J. Zimmerberg. 2003. Membrane permeability changes at early stages of influenza hemagglutinin-mediated fusion. *Biophys. J.* 85:1725–1733.
48. Shangguan, T., D. Alford, and J. Bentz. 1996. Influenza-virus-liposome lipid mixing is leaky and largely insensitive to the material properties of the target membrane. *Biochemistry.* 35:4956–4965.
49. Katsov, K., M. Muller, and M. Schick. 2006. Field theoretic study of bilayer membrane fusion: II. Mechanism of a stalk-hole complex. *Biophys. J.* 90:915–926.
50. Muller, M., K. Katsov, and M. Schick. 2003. A new mechanism of model membrane fusion determined from Monte Carlo simulation. *Biophys. J.* 85:1611–1623.
51. Nickel, W., T. Weber, J. A. McNew, F. Parlati, T. H. Sollner, et al. 1999. Content mixing and membrane integrity during membrane fusion driven by pairing of isolated v-SNAREs and t-SNAREs. *Proc. Natl. Acad. Sci. USA.* 96:12571–12576.
52. Dennison, S. M., M. E. Bowen, A. T. Brunger, and B. R. Lentz. 2006. Neuronal SNAREs do not trigger fusion between synthetic membranes but do promote PEG-mediated membrane fusion. *Biophys. J.* 90:1661–1675.
53. Chen, X., D. Arac, T. M. Wang, C. J. Gilpin, J. Zimmerberg, et al. 2006. SNARE-mediated lipid mixing depends on the physical state of the vesicles. *Biophys. J.* 90:2062–2074.
54. Deverall, M. A., E. Gindl, E. K. Sinner, H. Besir, J. Ruehe, et al. 2005. Membrane lateral mobility obstructed by polymer-tethered lipids studied at the single molecule level. *Biophys. J.* 88:1875–1886.
55. Tareste, D., J. Shen, T. J. Melia, and J. E. Rothman. 2008. SNAREpin/Munc18 promotes adhesion and fusion of large vesicles to giant membranes. *Proc. Natl. Acad. Sci. USA.* 105:2380–2385.